Bioorganic & Medicinal Chemistry 18 (2010) 7773–7785

Contents lists available at ScienceDirect

Bioorganic & Medicinal Chemistry

journal homepage: www.elsevier.com/locate/bmc

Ligand-based virtual screening and ADME-tox guided approach to identify triazolo-quinoxalines as folate cycle inhibitors

Emanuele Carosati [a], Gianluca Sforna [b], Massimiliano Pippi [b], Gaetano Marverti [c], Alessio Ligabue [c], Davide Guerrieri [c], Sandra Piras [d], Giambattista Guaitoli [e], Rosaria Luciani [e], Maria Paola Costi [e], Gabriele Cruciani [a,*]

[a] Dipartimento di Chimica, Università degli Studi di Perugia, Via Elce di Sotto 10, 06123 Perugia, Italy
[b] Molecular Discovery Limited, 215 Marsh Road, Pinner, Middlesex, London HA5 5NE, United Kingdom
[c] Dipartimento di Scienze Biomediche, Università degli Studi di Modena e Reggio Emilia, Via Campi 287, 41126 Modena, Italy
[d] Dipartimento Farmaco Chimico Tossicologico, Università di Sassari, Via Muroni 23/a, 07100 Sassari, Italy
[e] Dipartimento di Scienze Farmaceutiche, Università degli Studi di Modena e Reggio Emilia, Via Campi 183, 41126 Modena, Italy

ARTICLE INFO

Article history:
Received 6 June 2010
Revised 20 September 2010
Accepted 24 September 2010
Available online 1 October 2010

Keywords:
Folate cycle inhibitors
Triazolo-quinoxalines
Ligand-based virtual screening
FLAP
Ovarian carcinoma cell lines

ABSTRACT

In the process of drug discovery the lead-identification phase may be critical due to the likely poor safety profile of the candidates, causing the delay or even the abandonment of a certain project. Nowadays, combining molecular modeling and in vivo cellular evaluation can help to identify compounds with an enhanced safety profile. Previously, two quinoxalines have been identified as inhibitors of the folate-dependent proteins belonging to the thymidylate synthase cycle. Unfortunately, cytotoxic activity against a panel of cisplatin(cDDP)-sensitive ovarian carcinoma cell lines and their resistant counterparts was coupled with toxicity to non-tumorigenic Vero cells. Here we describe the application of a ligand-based virtual screening, and several [1,2,4]triazolo[4,3-*a*]quinoxalines were optimized to improve their ADME-tox profile. The resulting 4-(trifluoromethyl)-1-*p*-tolyl-[1,2,4]triazolo[4,3-*a*]quinoxaline (**24**), which interferes intracellularly with DHFR and TS reducing the protein levels like 5-FU, but without inducing TS ternary complex formation, was 2-times less toxic in vitro than cisplatin and 5-FU.

1. Introduction

The identification of a lead compound is a critical step in the process of drug discovery. The efficacy of anticancer drugs is usually accompanied with severe toxicity and the balance of these two biological effects is one of the most challenging problems in this area. Combining computational chemistry and in vitro cellular evaluation can lead to compounds with both an improved efficacy and safety profile (although it is well-known that simple cellular assays will not necessarily reveal all of the likely toxicities of a compound), therefore we applied this strategy to the ovarian cancer anticancer lead discovery process. Ovarian cancer is the most common cause of death from gynecological cancers among women of all ages in the western world. Efforts to improve survival continue to focus on the development of more effective systemic therapies.[1] Among these, the combination of cyclophosphamide or paclitaxel and a platinum compound such as cisplatin (cDDP) or carboplatin still represents the best available therapy in the standard treatment for this disease.[2] The use of drug combination therapy is justified by the occurrence of resistant cell populations in the tumor, which limit the usefulness of the platinum drug. Many studies have implicated an interaction between cisplatin and folate metabolism in the mechanism of resistance to cDDP, associated with cross-resistance to the folate antimetabolite methotrexate (MTX) in different tumor cell lines.[3–13] These cancer cells overexpress Thymidylate Synthase (TS) and dihydrofolate reductase (DHFR) and are intrinsically resistant to known therapeutic antifolates such as Pemetrexed and antimetabolites such as 5-fluorouracil (5-FU).[3–16] Both TS and DHFR are involved in the folate cycle: TS catalyzes the reductive methylation of deoxyuridine monophosphate (dUMP) by *N*-5,*N*-10-methylentetrahydrofolate (mTHF) generating dTMP and dihydrofolate,[17] and DHFR catalyzes the reduction of the dihydrofolate to tetrahydrofolate (THF) to provide new substrate material for the TS cycle. Since

Abbreviations: MTX, methotrexate; TS, thymidylate synthase; 5-FU, 5-fluorouracil; cDDP, cisplatin; dUMP, deoxyuridine monophosphate; dTMP, deoxythymine monophosphate; TSS, translational start site; mTHF, *N*-5,*N*-10-methylentetrahydrofolate; THF, tetrahydrofolate; TMQ, Thymitaq; PTX, Piritrexim; DHFR, dihydrofolate reductase; PSA, polar surface area; ADME, absorption, distribution, metabolism, excretion; PCA, principal component analysis; FLAP, fingerprint for ligands and proteins; MIF, molecular interaction fields.

* Corresponding author. Tel.: +39 075 585 5550; fax: +39 075 45646.
E-mail address: gabri@chemiome.chm.unipg.it (G. Cruciani).

0968-0896/$ - see front matter © 2010 Elsevier Ltd. All rights reserved.
doi:10.1016/j.bmc.2010.09.065

these enzymes are indispensable in the de novo synthesis of dTMP, playing an important role in DNA replication and repair in actively dividing cells, they have been attractive targets for anticancer chemotherapy. A large panel of human ovarian carcinoma cell lines, in which cDDP-resistance was associated with cross-resistance to 5-FU and MTX, showed an increase in TS and in the intracellular pools of mTHF and THF.[3]

Classic TS cycle inhibitors, such as 5-FU and MTX, are structurally similar to the substrate and the co-substrate, respectively. However, this chemical structure resemblance has often induced resistance in vivo and in many cell lines in vitro; therefore, new drugs must be developed to avoid this resistance.[18]

With the aim of designing new molecules able to overcome resistance by interfering with the folate cycle as in previous studies, structural elaboration of the classical pteridine core led to the identification of the quinoxaline nuclei as an interesting core scaffold.[19] The pteridine moiety present in the most active anticancer agents (MTX, TMQ and PTX) was then replaced with this quinoxaline ring functionalized with the trifluoromethyl and/or amino group. Such modifications bioisosterically modulated the affinity for DHFR and TS enzymes.[19] In particular, several substituents often present in classical and non-classical antifolates were inserted at positions 2 and 3 of the quinoxaline ring (see Chart 1). Among them some 3-parasubstituted-benzoyl and 2-piperazinyl quinoxalines were found to inhibit TS and DHFR and demonstrated anticancer activity,[19] exhibiting low values of cytotoxicity in the anticancer test performed at the National Cancer Institute. Two quinoxalinic compounds were identified with interesting activities at the cellular level,[20] namely 3-phenyl-7-(trifluoromethyl)-*N*-(3,4,5-trimethoxyphenyl)quinoxalin-2-amine (**1**), previously named as 453R and (4-methoxyphenyl)(3-(4-methylpiperazin-1-yl)quinoxalin-2-yl)methanone (**2**), previously named as 311S.[20]

Two human ovarian carcinoma cell lines, 2008 and A2780, and the corresponding cisplatin-resistant sublines C13* and A2780/CP were used, whereas the Vero lineage was chosen as control cell line. Vero cells are normally used as control cells[21] because they present very well defined properties which enable easy observations of possible growth modification by chemical agents. The rationale behind the use of Vero cells rather than primary ovarian cells is that these cells can be banked and well characterized. This avoids the issue of lot-by-lot variability and adventitious agent contamination of primary cultures freshly initiated for each study from the ovaries of patients. In addition, this line shares a common embryonic origin (mesoderm) with cells from the human genital tract,[22] and it is recommended for investigation in standard protocols (ISO 10993-5, 1992-E). Despite the weak inhibitory potency at the enzyme level (hTS, K_i 125 μM and 10% inhibition of hDHFR at 50 μM for compound **2** and 10% inhibition at 50 μM for compound **1** against hTS and no inhibition of hDHFR), these molecules showed a modulation of the cell cycle through the reduction of TS and DHFR protein expression and the effective capacity to restore the sensitivity to cisplatin drug in cisplatin-resistant cells; therefore they were defined as folate cycle inhibitors.[20]

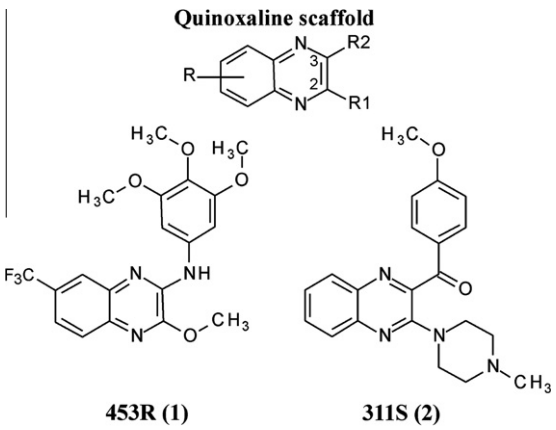

Chart 1. Quinoxalines inhibitors of the folate cycle.

The cisplatin-resistant line, C13* cells, exhibited a 2- and 2.3-fold collateral sensitivity towards **1** and **2**, respectively, when compared to its sensitive parental 2008 cells. In this resistant line, which showed elevated expression of TS and DHFR due to cisplatin-resistance phenotype, collateral sensitivity correlated with the greater reduction of enzyme expression. In addition, median effect analysis of the interactive effects of cisplatin with the two quinoxalines mainly showed additive or synergistic cell killing, depending on schedules of drug combinations.[20] More recently, it has been shown that the simultaneous combination with polyamine analogues of quinoxalines **1** and **2** or their pre-treatment synergistically increased spermidine/spermine *N*1-acetyltransferase (SSAT) expression, depleted polyamines, increased reactive oxygen species (ROS) production, and produced synergistic tumor cell killing in both 2008 and C13* cell lines. This combined therapy increased the chemosensitivity of cisplatin-resistant cells and cross-resistant to the polyamine analogues. On the contrary, some pre-treatment regimens of spermine analogues were antagonistic.[23]

Being quinoxalines multitarget compounds, since they are well-known DNA binders, c-Met inhibitors and Topoisomerase inhibitors,[24] off-target effects may be an issue, with toxicity remaining a critical aspect. Thus, the control of the multitargeting, by impairing the toxic effect from the pharmacological activity, could improve the biological profile of compounds **1** and **2**.

In this context, we adopted a ligand-based virtual screening approach starting from the aforementioned quinoxalines **1** and **2**. A library of approximately eleven thousand quinoxaline-containing compounds was extracted from the ZINC archive,[25,26] containing either the quinoxaline moiety itself or included in a larger cyclic system. Among the filters used in the screening, as well as in the later refinement procedure, ADME properties were predicted in silico for the compounds of the library; properties such as molecular weight, predicted aqueous solubility, and calculated polar surface area (PSA) have been often used in screening processes to prioritize compounds.[27] Their use as computational filters allowed the selection of a reduced set of molecules to be compared with the two reference molecules **1** and **2** by means of a pharmacophore-based method recently developed for virtual screening purposes.[28,29]

Investigating other compounds via classic structure–activity relationships of the novel hits found allowed the collection of a subset of analogues with significant differences in activity and toxicity. By studying such differences and combining with ADME-tox prediction, enzyme profiling and cellular studies, compounds with an improved predicted profile of high-activity/low-toxicity were designed and compounds with higher activity and lower toxicity with respect to the existing drugs (FU, taken as a reference) were identified. The entire procedure of the identification via ligand-based virtual screening and the ADME-tox optimization are described in this paper.

2. Results

2.1. Ligand-based virtual screening

2.1.1. Overview

The ligand-based procedure was applied to the release 5 of the ZINC database supplied via the worldwide web,[25] which contained roughly 3,000,000 commercially available compounds. The ZINC database[25] provides files corresponding to substances distributed from different vendors,[26] and the entire database was processed

by using the SMILES compounds' codes.[30,31] Among this large set of compounds the quinoxaline scaffold was found only in approximately eleven thousand compounds, which were further investigated.

The main focus of a virtual screening procedure is to reduce the size of a chemical library, providing a focused subset of molecules, enriched in compounds likely to be active, which are then screened experimentally. A multi-step process was applied: the schema of the screening procedure is presented in Figure 1, whereas each single step is described below.

2.1.2. Pharmacokinetic filtering

A preliminary analysis of data from Ref. 19 suggested pharmacokinetic properties such as molecular weight (MW), aqueous solubility (SOLY) and polar surface area (PSA) as filters for reducing the database. An initial set of 10,745 compounds was reduced to only 1568 molecules by using criteria based on the mentioned molecular properties, calculated using the VOLSURF+ molecular descriptors.[32–34]

Initially, compounds with MW between 300 and 450 were retained; then, compounds with the SOLY value between −5.5 and −4.0 were further analyzed; finally, only compounds with PSA <80 reached the final step.

At the end of this process the database size was significantly reduced from 10,745 to 1568, which equals an elimination of about 89%. In brief, according to the filters used, the compounds of this selection are of 'medium-size' with a large hydrophobic moiety.

2.1.3. FLAP similarity

These 1568 compounds were in turn investigated using similarity measures calculated with the FLAP program,[28,29,35] a recently developed algorithm which has been previously used successfully on structure-based (high-throughput virtual screening of proteins)[36] and ligand-based projects such as virtual screening,[37,38] QSAR[39] and pharmacophore hypothesis generation.[40,41] FLAP is well suited for describing objects (proteins and/or ligands) on the basis of a common reference framework. In this ligand-based case, compounds **1** and **2** were used as reference templates whereas the 1568 quinoxaline-containing compounds constituted the so-called 'ligand molecules'.

FLAP aligns two molecules and quantifies the similarity between them. The 'ligand molecule' is aligned with each 'template molecule', that is the reference, using pharmacophoric similarity. A FLAP pharmacophore, which will be referred to as 'quadruplet', is a combination of four hotspots (molecular atoms): each quadruplet of the ligand is searched over each of the template quadruplets. For each match, that is obtained when four hotspots of the ligand molecule are found to fit over four hotspots of the template, a potentially favorable superposition is detected. This iterative process continues until all of the template quadruplets are combined in all possible ways with all ligand quadruplets. Each time, a score associated to the 3D-superposition of the two molecules, resulting from the alignment of their corresponding quadruplets, quantifies the 3D-similarity. At the end of the process, only the best score obtained, that corresponds to the best superposition of each ligand to the template is used to assess the 3D-similarity between the two molecules. The FLAP score is an estimation of how the Molecular Interaction Fields (MIF) calculated for the two molecules with the GRID force-field[42–44] are intersected. Since the MIF encode into energy values the information of hydrophobic and hydrogen bonding interactions of the molecule with a virtual receptor, the best intersection of the MIF of two molecules represents the interaction with a virtual receptor that potentially the two molecules have in common.

The screening was performed using the set of 1568 compounds, and for each compound the similarity versus the templates **1** and **2** was calculated. Compounds with high similarity to at least one template were checked for chemical instability and/or potential toxicity by visual inspection: removing compounds with potential toxic and/or reactive functional groups was based on literature suggestions[45,46] and basic medicinal chemistry criteria. Finally, the availability was checked from the vendor databases and 14 compounds were purchased. These compounds, identified by virtual screening and biologically tested, are reported in Chart 2.

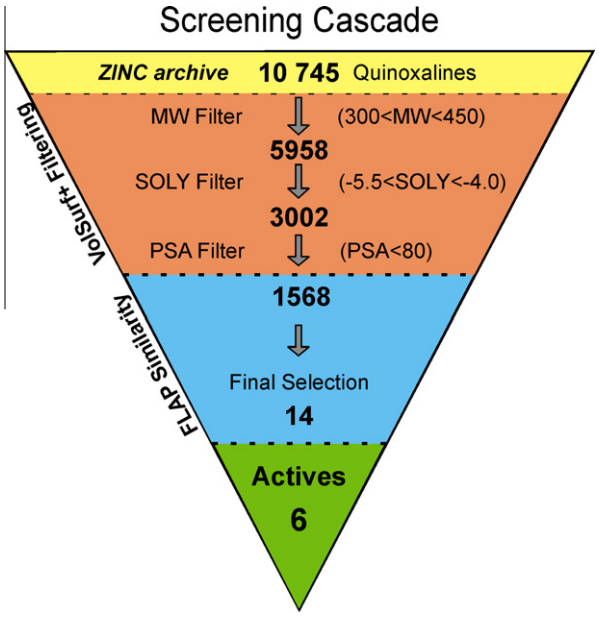

Figure 1. The ligand-based virtual screening (LBVS) cascade. Pharmacokinetic filtering via VOLSURF+ reduced the initial database of 10,745 structures to a set of 1568 compounds. Similarity scores were calculated with the FLAP method using the two reference compounds **1** and **2** as templates. In this way, 14 compounds were selected. Biological tests on human ovarian cancer cell lines yielded six active compounds.

2.2. Analysis of potential inhibitors

The compounds that showed interesting cell growth inhibitory activity against ovarian cancer cells were considered as hits; their data are graphically reported in Figure 2 in comparison with some references (cDDP, 5-FU, **1** and **2**). All the selected compounds, given their structural diversity, are discussed below on the basis of the quinoxalinic scaffold, using the groups presented in Chart 2.

Four compounds are basically quinoxalines, differently monosubstituted at positions 6 (**3**, **4**, and **5**) or bi-substituted at 2 and 3 (**6**). Overall, this group was the least interesting since two compounds, **5** and **6**, resulted insoluble whereas the other two, **3** and **4**, for which the experiments were conducted, were inactive.

Four other compounds have a tri-cyclic, quinoxaline-containing, scaffold. Both compounds **7** and **8** are [1,2,4]triazolo[4,3-*a*]quinoxalines substituted at position 4, but **7** is also substituted with *p*-chlorophenyl at position 1. This scaffold was very promising, given the activity of **7** and **8** on 2008 and C13* cells. In particular, compound **8** was weakly active and with a scant selectivity for the cell lines used, having IC_{50} values of 17 μM on 2008 cells, 19 μM on C13* cells, and 20 μM on Vero cells, whereas **7**, namely 1-(4-chlorophenyl)-4-trifluoromethyl-[1,2,4]triazolo[4,3-*a*]quinoxaline (LQ011), was the most potent of the series on both 2008 and C13* cell lines, with IC_{50} values of 2.5 μM on 2008 cells and 3.4 μM on C13* cells, respectively. Also **7** was not selective, being active and even more potent on Vero cells with IC_{50} value of 1.2 μM. The other tri-cyclic scaffolds were 1*H*-pyrrolo[3,2-*b*]quinoxaline **9** and 1*H*-imidazo[4,5-*b*]quinoxaline **10**. Of these two compounds, **9**

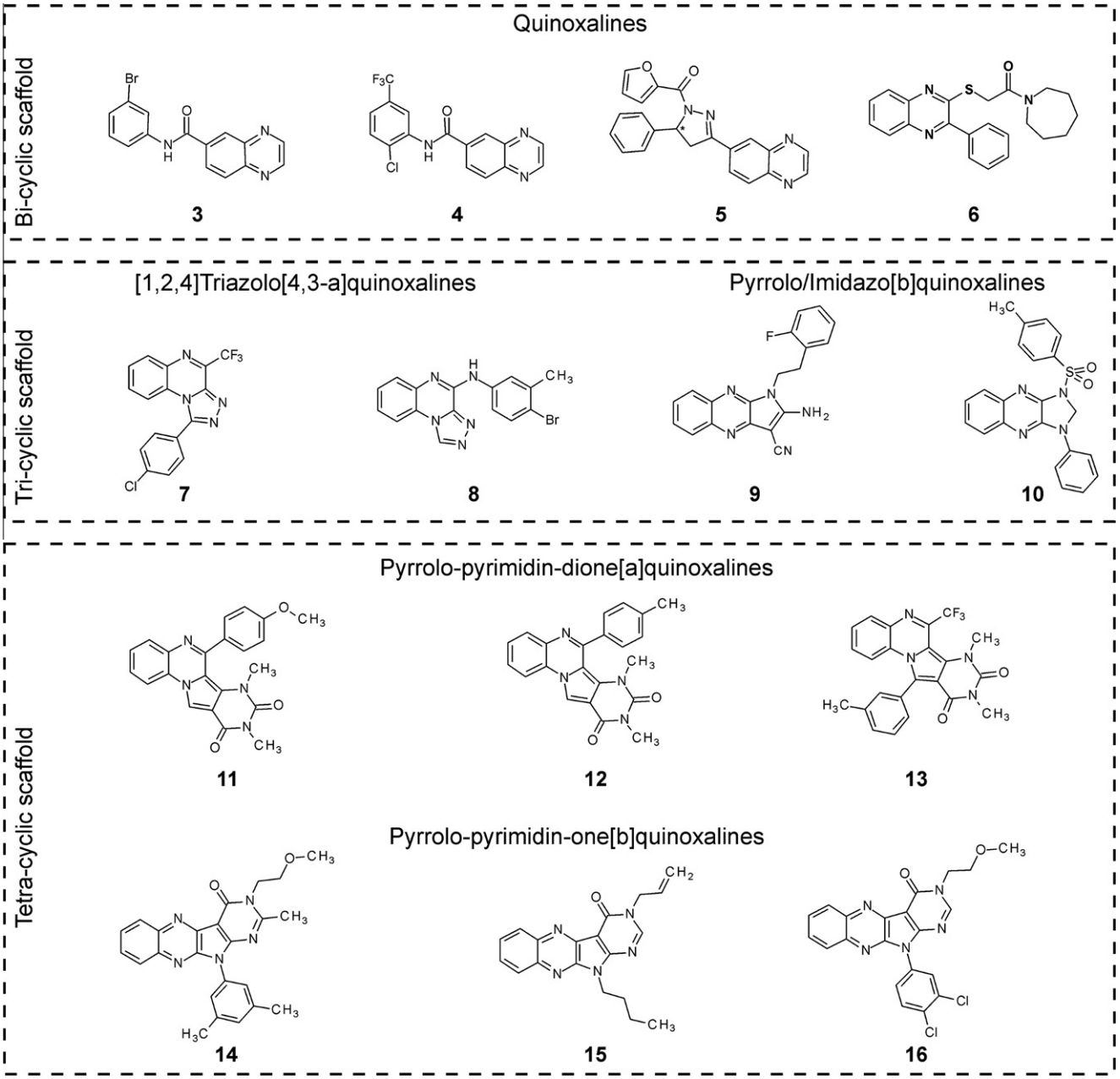

Chart 2. Structures of the compounds identified by virtual screening (compound **5** was purchased as racemate).

and **10**, which differ for the five-member ring and for their substituents, only **9** was active, with IC_{50} values of 18 μM on 2008 cells and 22 μM on C13* cells, but also 9.1 μM on Vero cells, presenting the problem of low selectivity and cell toxicity like **7**. The dihydro-1*H*-imidazo-quinoxaline compound, **10**, was inactive.

Six tetra-cyclic compounds were selected via virtual screening and purchased, but three out of six resulted insoluble in DMSO. The three that were experimentally tested, **12**, **13**, and **16**, were slightly active on both the ovarian carcinoma cell lines, being the IC_{50} in the range of 30 μM (**16**) or 50 μM (**12** and **13**), and selective, being the IC_{50} for Vero cells greater than 50 μM for **16** and than 100 μM for **12** and **13**. For two 1,3-dimethyl-1*H*-pyrrolo [3,4-*d*]pyrimidine-2,4(3*H*,6*H*)-diones (**12** and **13**) the same substituent, the tolyl group, is differently linked to the quinoxaline (**12**) and pyrrolo (**13**) moieties, whereas for **16** a di-chloro-phenyl group is linked to the tetra-cyclic structure.

Given the problematic solubility range of the starting quinoxalines **1** and **2**, low soluble derivatives were expected. This problem affected also the in vitro experiments with hTS: compounds **11**, **12**, **14**, **15**, and **16** were not soluble in DMSO and could not be tested whereas compounds **3**, **4**, **6**, **8**, **9**, **10**, **11**, and **13** were not inhibitors at 50 μM, and **5** at 100 μM. Summarizing, nine compounds were tested but none inhibited hTS at the concentration used (up to 50–100 μM).

At the cellular level the situation was more promising, since nine compounds were tested and six out of nine killed tumor cells in a range of 50 μM (Fig. 2). Unfortunately, the most potent hits found (**7**) revealed a scant selectivity of action because it inhibited the growth of the Vero cells in the same range as the effective inhibitory concentration, whereas the less potent compounds were more selective. Four different quinoxaline-containing scaffolds were identified as active for inhibiting the folate cycle. Two of

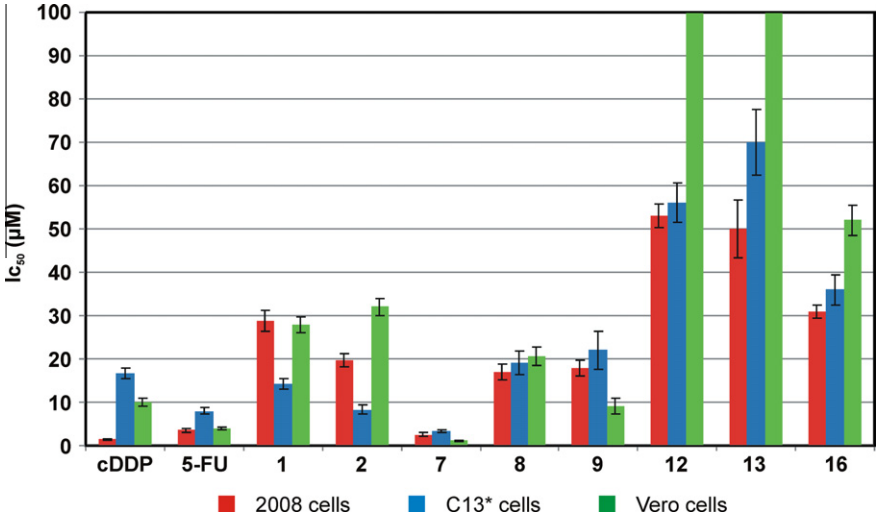

Figure 2. IC_{50} values (μM) against the human ovarian 2008 and C13* cell lines, and against Vero lineage for the reference compounds (cDDP, 5-FU, **1** and **2**) and for the hits identified with the virtual screening **7**, **8**, **9**, **12**, and **13** and **16**.

them, the [1,2,4]triazolo[4,3-*a*]quinoxaline scaffold of the hits **8** and **7**, and the 1*H*-pyrrolo[3,2-*b*]quinoxaline scaffold of the hit **9**, are tri-cyclic whereas the other two, the pyrrolo-pyrimidin-dione[*a*]quinoxaline and pyrrolo-pyrimidin-one[*b*]quinoxaline scaffolds, are tetra-cyclic. Only one scaffold (the [1,2,4]triazolo[4,3-*a*]quinoxaline) was selected for further investigation, by studying a few derivatives as described in the next section. Data of the activity on 2008, C13* and Vero cell lines is also reported in the Supplementary data.

2.3. Derivatives of novel folate cycle inhibitors

The two molecules with the [1,2,4]triazolo[4,3-*a*]quinoxaline core, **7** and **8**, were among the most promising in terms of potency, with **7** being the most effective drug, with interesting IC_{50} values (2.5 and 3.4 μM) in 2008 and C13* cells as well as against Vero cells (1.2 μM). With the aim of reducing the toxic effect from the pharmacological activity and to shed light on the biological behavior of this class of compounds, six new derivatives of **7** were found by searching through the initial quinoxaline-dataset, and their effect was studied on both enzyme hTS and cells. The structure of the selected derivatives is presented in Chart 3, the biological activities are reported in Table 1 and the structure–activity relationships are briefly discussed below.

At the cellular level, the only active derivative out of these six was **17**, with IC_{50} values of 17.5 μM (2008 cells) and of 27 μM (C13* cells). Unfortunately, **17** was still more potent on Vero cells, with IC_{50} of 14 μM. Among the inactive derivatives **19** can be mentioned, since its activity, limited to the 2008 cell line with IC_{50} of 48 μM, resulted much lower than its toxic effect on the safe cell, with an IC_{50} on Vero cells of 22 μM. Summarizing the structure–activity relationships observed so far, no optimization of the activity versus the toxicity was achieved. However, all the collected data, taken together, could be used for building qualitative models to be used in the design of more selective compounds, as described in the next section.

At the enzymatic level (see Table 1), two of the six derivatives (**21** and **22**) revealed interesting activity, with 53% of inhibition at 25 μM (**21**) and 70% of inhibition at 50 μM (**22**). Another three compounds were slightly active (**17**, **18** and **20**) whereas the remaining one (**19**) was almost inactive. The inhibition of the TS enzyme does not parallel the cellular inhibitory activity and this may be due to difficulties in membrane crossing. Despite the low potency in the enzymatic test (Table 1), compound **19** was passed to the cellular assay because the piperazinyl ring is usually considered a fragment that improves the solubility and cellular membrane permeability.

2.4. ADME-tox optimization of [1,2,4]triazolo[4,3-*a*]quinoxaline derivatives

The biological activities on the three cell lines (2008, C13* and Vero) were available for eight compounds (**7**, **8**, **9**, **12**, **13**, **16**, **17**, and **19**). A PLS2 model was built over this set of molecules with VOLSURF+ to investigate the relationships between the activities on 2008 and C13* cell lines and the toxicity, the latter being the activity on the Vero cells. Given the extremely low number of compounds used, these models were developed for interpretative purposes only.

The PLS2 method reports three separate PLS models for the three activities (Fig. 3a) but also an overall model for the relationships between the blocks X and Y. In the resulting plot of PLS weights (Fig. 3b) it is evident that the activities on 2008 and C13* cells are coupled, whereas the activity on the Vero cells (toxicity) is more isolated. Being the final aim of this optimization the reduction of such toxicity without affecting the other activities, the PLS coefficients (Fig. 3c) were analyzed to identify which variables (molecular descriptors) could be easily modulated in order to decrease the activity on Vero cells.

The metabolic stability (MetStab VOLSURF+ descriptor) was selected as the molecular descriptor, directly related to the cellular toxicity, to be reduced in order to decrease the activity on Vero cells (i.e., reduce the toxicity). The presence in cancer cells of defensive/detoxifying enzymes such as cytochromes P450 has been investigated by several authors. In particular, the expression in malignant cells of enzymes of the subfamily 1A has been reported[47,48] and recently reviewed.[49] Therefore, following this hypothesis, new derivatives of **7** (LQ011) were designed focusing on the reduction of their (predicted) metabolic stability, by changing a metabolically stable group with a more unstable group.

The design of new derivatives of **7** was carried out with the help of the program MetaSite,[50,51] used to predict the metabolism of **7**. METASITE was specifically designed to study the metabolism of xenobiotics due to cytochromes P450, and to predict the sites of metabolism (SOM). The predictions obtained with MetaSite for **7** are reported in Figure 4: the first two solutions (most unstable groups)

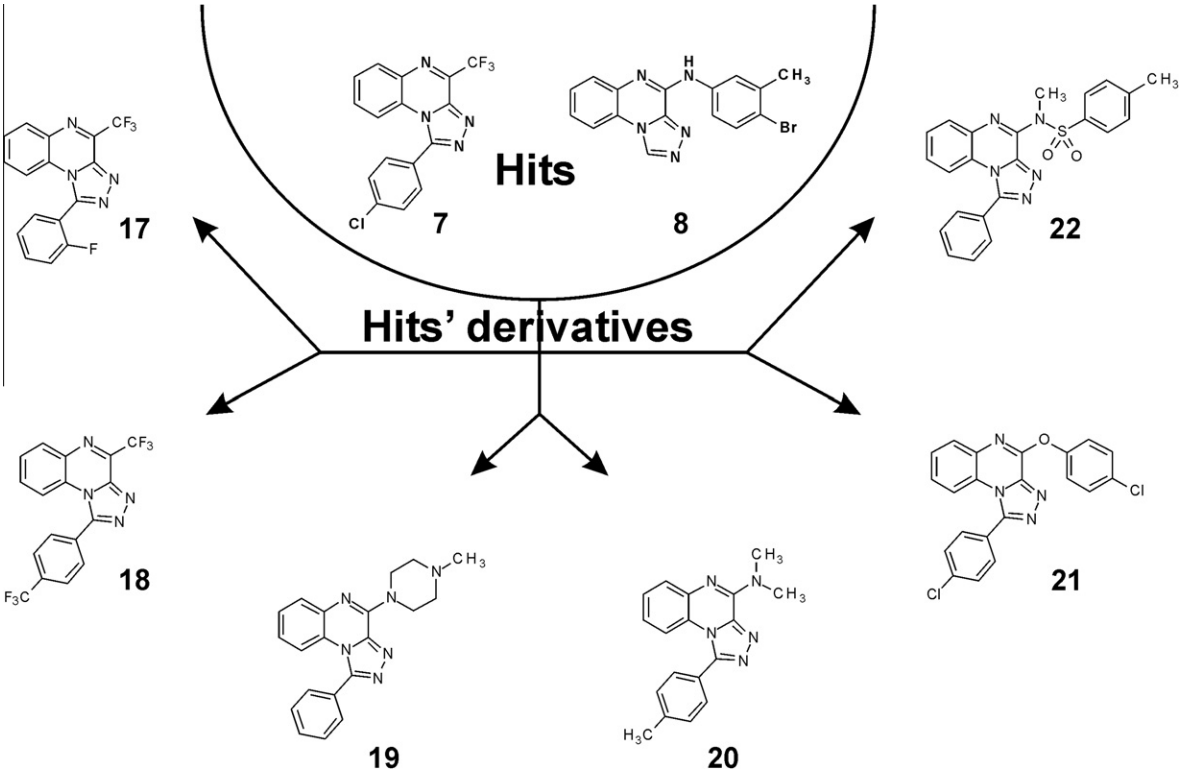

Chart 3. Structures of the hits' derivatives starting from compounds **7** and **8**.

Table 1
TS and DHFR inhibitory activity at 100 μM and IC_{50} values (μM) for the triazoloquinoxaline **17**–**22** against the human ovarian 2008, C13*, and Vero lineages

	TS% inhib (100 μM)	DHFR% inhib (100 μM)	IC_{50} (μM) 2008 cells	IC_{50} (μM) C13* cells	IC_{50} (μM) Vero cells
17	17	10	17.5	27	14
18	22	10	>50	>50	NT[a]
19	<10	40	48	>50	22
20	41	NI[d]	>50	>50	NT[a]
21	53[b]	NI[d]	>50	>50	NT[a]
22	70[c]	NI[d]	>50	>50	NT[a]

[a] NT = Not tested.
[b] 25 μM.
[c] 50 μM.
[d] NI = No inhibition.

are the quinoxaline ring (especially position 7 of [1,2,4]triazolo[4,3-*a*]quinoxaline) and the two positions (in *meta* with respect to the chlorine) of the phenyl ring which is substituted at position 1 (Fig. 4a).

The MetaSite prediction with the reactivity factor switched 'off' offers an alternative perspective. This way the researcher can investigate exclusively the affinity with the enzyme cavity of the different molecular moieties. This is often roughly referred to as the 'exposure' of the atoms/groups of the compound within the enzyme cavity.[52,53] In case of **7** the most exposed group is the phenyl ring at position 1, and in particular the chlorine atom (Fig. 4b). The designed molecules were subjected to metabolic stability and Met ID experiments, whose results will be reported in due course.

Overall, modifications at the *p*-chlorine group were expected to favor the metabolism, and three derivatives were designed with this scope. 1-(2,6-Dichlorophenyl)-4-methyl-[1,2,4]triazolo[4,3-*a*]quinoxaline (LQ029, **23**) differs from **7** for two chlorine atoms in *ortho*-position instead of one chlorine atom in the *para*-position (see Chart 4); in 4-methyl-1-(*p*-tolyl)-[1,2,4]triazolo[4,3-*a*]quinoxaline (LQ030, **24**) such chlorine atom is replaced by a methyl group, whereas 4-chloro-1-phenyl-[1,2,4]triazolo[4,3-*a*]quinoxaline (LQ031, **25**) is unsubstituted in the phenyl at position 1 and a chlorine atom replaces the trifluoromethyl group. The structures of **23**, **24** and **25** are presented in Chart 4, whereas their biological activities are reported in Table 2.

2.5. Biological activity of the optimized compounds

The cytotoxic effects of the most interesting compounds **7**, **23**, **24** and **25** have been compared with the dose–response curves of the traditional anticancer drugs cDDP and 5-FU (Fig. 5). The C13* cells, about 13-fold and 4-fold resistant to cDDP and 5-FU respectively, were almost as sensitive to **7** and **25** as 2008 cells, indicating that the pharmacology of these novel compounds was not affected by the resistance phenotype. On the contrary, even if the order of magnitude of the IC_{50} of **23** and **24** against the sensitive tumor cells is higher than the classical anticancer compounds, both **23** and **24** presented a higher cytotoxic activity towards the resistant line (Table 2).

The results on the other pair A2780-A2780/CP cell lines showed that there is no specific activity towards the resistant line, since the IC_{50} values of these compounds were quite the same in sensitive and resistant lines, especially with the compounds **23** and **24**. Interestingly, **24** and **25** showed a better selectivity than both traditional drugs and **7**, since they were less toxic against Vero lineage than the other drugs. In particular, compound **25** appeared the most interesting inhibitor of cell growth, even improved with respect to **7**. This result is even better if compared with the cytotoxicity against A2780 and A2780/CP, which were 7.3- and 3-fold, respectively, more responsive to **25** than the Vero lineage (Table 2). In addition, all drugs did not affect human fibroblast cell growth up to 100 μM (data not shown).

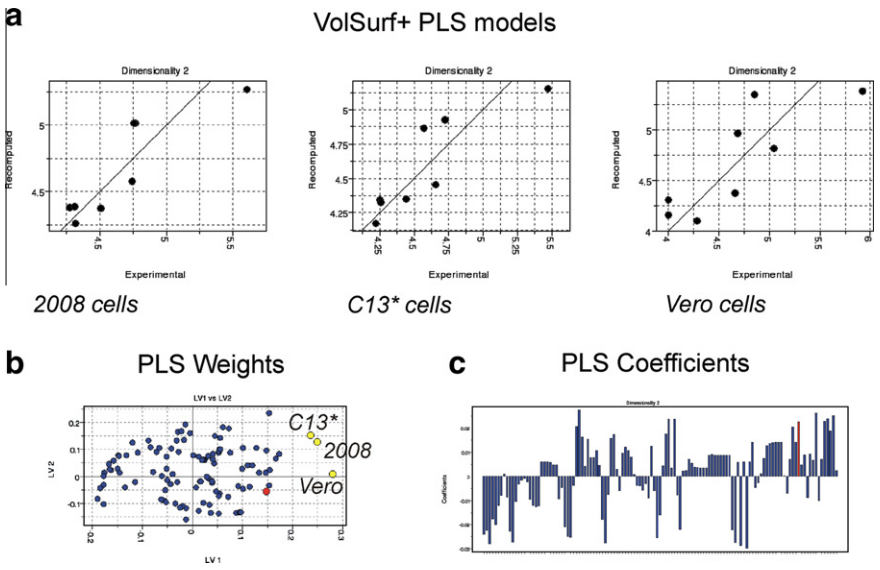

Figure 3. (a) VolSurf+ molecular descriptors are related to biological activities (expressed as pIC_{50}) on 2008, C13* and Vero cell lines via three separate PLS models. (b) Using the PLS2 method the three activities can be handled simultaneously: in the 'PLS Weights' plot the three dependent variables are reported with yellow circles, the molecular descriptors are reported with blue circles, whereas the descriptor MetStab is represented with the red circle. (c) PLS coefficients plot for the PLS model for the Vero cell line; the red bar in the histogram is the molecular descriptor named MetStab, which refers to human metabolic stability.

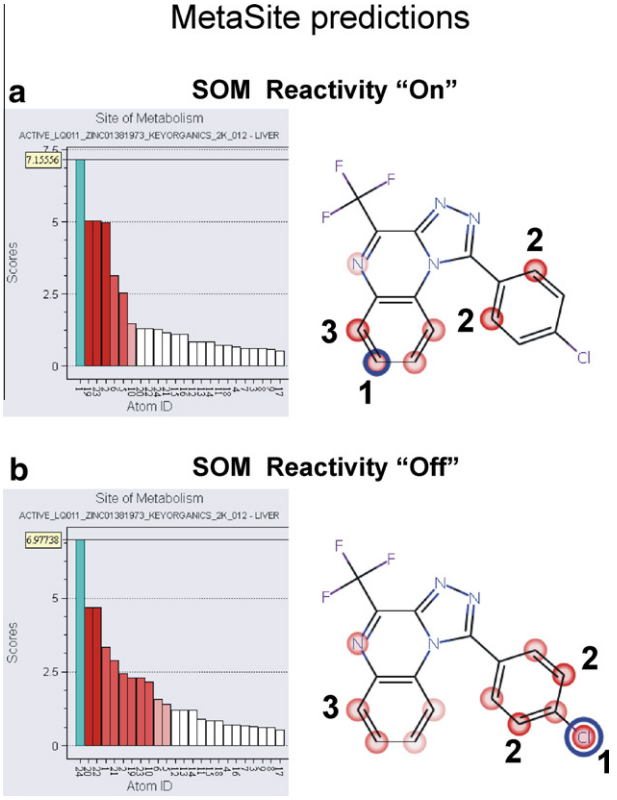

Figure 4. MetaSite predictions for **7** obtained with the reactivity switched 'on' (a) or switched 'off' (b). The first three sites of metabolism (SOM) are reported with the codes **1**, **2**, and **3**. The calculations were run using the 'liver' consensus model.

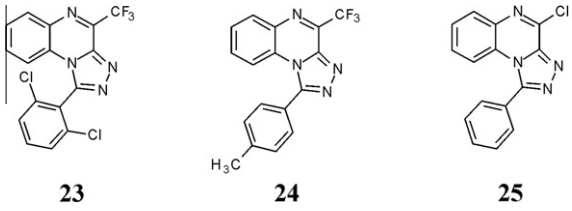

Chart 4. Structures of the compounds of the ADME-tox optimization.

Table 2
IC_{50} values (μM) for the references **1** and **2**, and triazolo-quinoxalines against cDDP-sensitive (2008, A2780) and resistant counterpart (C13*, A2780/CP) ovarian cancer cells and Vero lineage

	2008	C13*	A2780	A2780/CP	Vero
1[a]	28.8 ± 2.4	14.2 ± 1.3	27.5 ± 3	35.3 ± 4	40.2 ± 4.1
2[a]	18.8 ± 1.5	8.3 ± 1	17.4 ± 1.5	27.4 ± 2.6	42.4 ± 3.3
7	2.5 ± 0.4	3.4 ± 0.5	2.3 ± 0.4	4.7 ± 0.5	1.2 ± 0.2
17	17.5 ± 2	27 ± 3.1	9 ± 1.1	11 ± 1	14 ± 1.3
19	48 ± 4.5	>50	18 ± 2	38 ± 2.9	22 ± 1.5
23	37 ± 5	28 ± 2	27.5 ± 2.5	25 ± 2	10 ± 0.7
24	42.5 ± 2.5	26.7 ± 1	33 ± 1	35.7 ± 1.5	>50
25	12.5 ± 1	13 ± 1.2	2.5 ± 0.3	6 ± 0.5	18.2 ± 1.6

The IC_{50} is defined as the concentration causing 50% growth inhibition in treated cells when compared to control cells after 72-h drug exposure. Values are means ± S.E.M. of four separate experiments performed in duplicate. Exception is **25** for which $N = 5$.

[a] From Ref. 20.

The effects of two representative of the new compounds on folate cycle enzymes expression of 2008 and C13* cells have been verified. In particular, we have chosen **23** and **24** which showed a higher activity against resistant than sensitive cells but with a different selectivity towards the non-tumorigenic Vero line. Like the two quinoxalinic compounds **1** and **2**, compounds **23** and **24** induced a decrease in the TS expression (Fig. 6a). In particular, **24** induced a dramatic reduction of the amount of TS, which almost disappeared in the sensitive line and barely reaches 10% of control in the resistant one.

On the other hand, DHFR expression even showed a greater inhibition after exposure to **23** and **24**, and they were, like **1** and **2**, more active on the resistant line with respect to the sensitive one (Fig. 6b). Partly correlating with the effects on TS protein level, **23** and **24**, at their IC_{50} values, interfere with the catalytic activity of TS enzyme in both 2008 and C13* cell lines, after 72 h-treatment (Fig. 6c). Moreover, both **23** and **24**, accordingly to cytotoxicity, appeared to affect more specifically the resistant line (32.3 ± 0.9

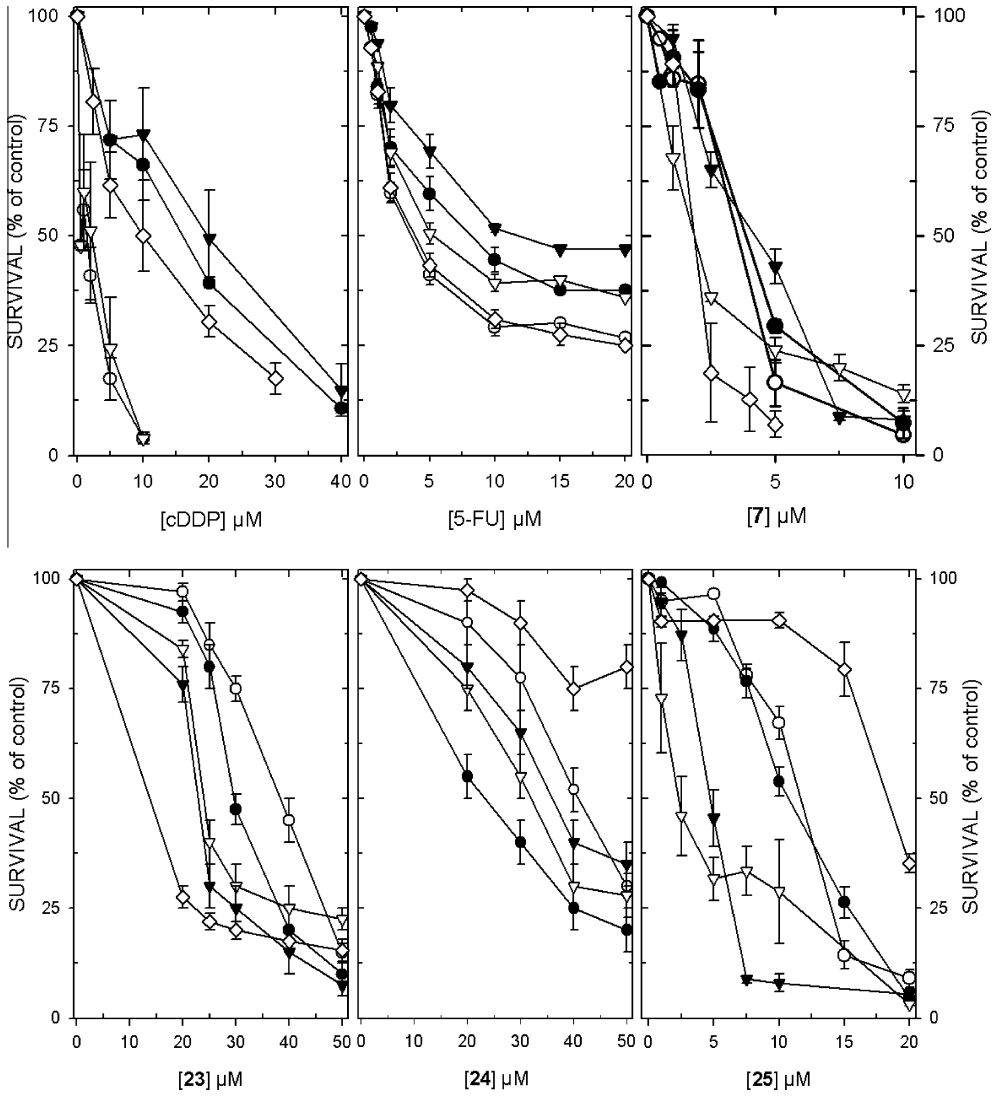

Figure 5. Dose–response curves of cDDP, 5-FU, **7**, **23**, **24** and **25** against human ovarian cancer cell lines and Vero lineage. 24 h after seeding, 2008 (open circles), C13* (closed circles), A2780 (open triangle down), A2780/CP (closed triangle down) and Vero (open diamonds) cell lines were exposed to the indicated concentrations of the drugs for 72 h and then fixed and stained with crystal violet solution. Results represent the mean of three separate experiments performed in duplicate. Error bars, S.E.M.; where not visible, error bars did not exceed symbol size.

and 12.9 ± 0.6% of control, respectively) than the sensitive line (58.9 ± 3.6 and 38.8 ± 3.9, respectively).

Compounds **23** and **24** did not show any activity against TS enzymes at concentration lower than 50 μM due to solubility limit, whereas **25** showed inhibitory activity of 28% at 50 μM hTS (K_i estimated at 10 μM). In general, it was not possible to test the compounds at concentration higher than 50 μM due to solubility limit. However, the inhibitory effect of the TS protein observed in the cellular extract (Fig. 6) is likely due not only to the inhibition of the TS protein itself, but also to the lower protein concentration in the cells when the cells are pre-treated with the compounds, suggesting the occurrence of an inhibition either at transcriptional or post-transcriptional level.

Apart from the folate cycle inhibition activity, the quinoxalinic compounds may act with other mechanisms, since exogenous compounds may oxidize intracellular products producing hydrogen peroxide, which at high levels damages mitochondrial membranes and triggers the cascade to apoptosis.[54] Thus, we checked for quinoxalines-induced production of Reactive Oxygen Species (ROS) by means of the fluorescent probe CM-H2DCFDA. Indeed, results from our study show that these novel folate cycle inhibitors elevate cellular hydrogen peroxide content, which may initiate the apoptotic cascade. However, this effect does not appear to contribute to the cell growth inhibition in resistant cells since ROS production was comparable to controls. Probably, the more elevated content of intracellular detoxifying compounds such as metallothionein, glutathione and thioredoxin,[55] allows resistant C13* cells to counteract the toxic effects better than sensitive 2008 line (see Supplementary data).

3. Discussion and conclusion

The up-regulation of folate cycle enzymes is probably the most common mechanism of resistance presented by a wide panel of cisplatin-resistant human tumor cell lines, including ovarian carcinoma cells[3] such as the C13* and A2780/CP cells used in this study. By this mechanism resistant cells can survive better the drug injury caused by cDDP or by other traditional TS inhibitors such as 5-FU.

Therefore, the development of treatments against tumor cells resistant to TS inhibitors, without the concomitant long-term over-expression of folate cycle enzymes, appears nowadays of great importance. In this context we have recently reported two

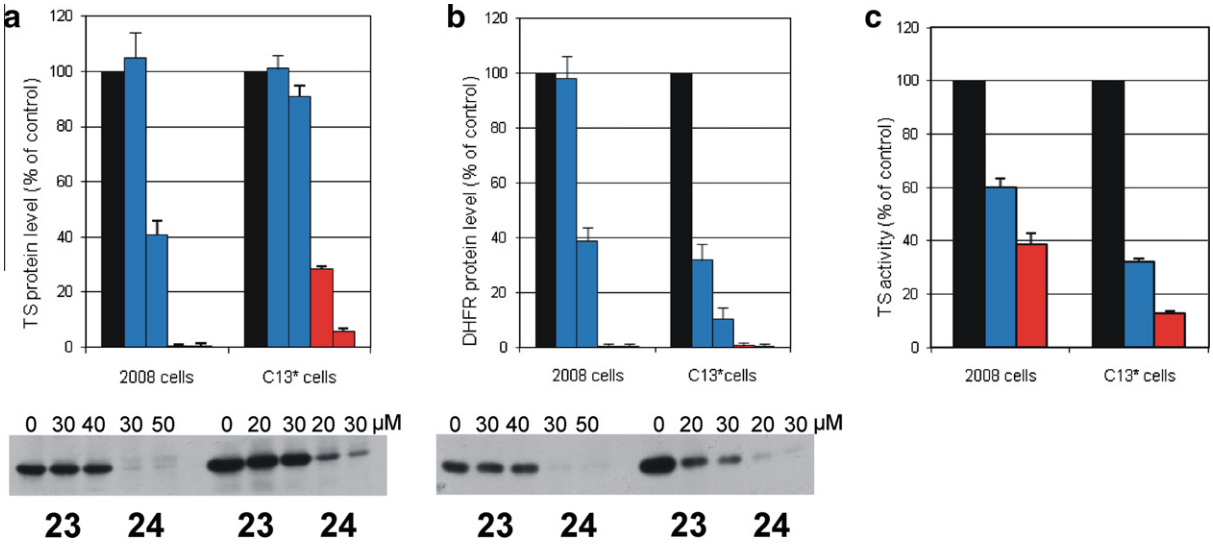

Figure 6. Effects of **23** and **24** on TS and DHFR expression in 2008 and C13* cells. (a and b) Western immunoblot analysis of TS and DHFR from 2008 and C13* cells treated for 72 h with the indicated concentrations of **23** (blue bars) and **24** (red bars). The blots of hTS monomer, molecular mass of 35 KDa, and DHFR monomer, molecular mass of 21 KDa, were quantified by densitometric scanning and the values were bar graphed. Western blot analyses were performed on cytosolic extracts from cells in the exponential phase of growth and prepared as described in Section 4, using an anti-human TS and DHFR monoclonal antibody. Results of a typical experiment, which was carried out three times, are shown. Equal lane loading was confirmed using an anti-human β-tubulin mouse antibody (β-tubulin protein level did not change significantly and it was not shown). (c) TS activity inhibition in 2008 and C13* cells was determined under the same experimental conditions using the IC_{50} values of **23** (blue bars) and **24** (red bars) for 72 h. Results represent the mean of three separate experiments performed in duplicate. Error bars, S.E.M.

quinoxalines **1** and **2** able to inhibit the expression of both TS and DHFR, and in particular of a cDDP-resistant human ovarian carcinoma cell line. Starting from the quinoxaline core structure of compounds **1** and **2**, in silico ADME predictions were applied in parallel with enzyme profiling and cellular growth inhibition (cytotoxicity) to understand how to progress along the optimization stage. In this case we considered as important activity indicator the cellular activity of the compounds with respect to enzyme inhibition, because we have observed that even the references **1** and **2** were folate cycle inhibitors with low efficacy against the recombinant protein. A set of 14 compounds was selected starting from a large database of approximately eleven thousand quinoxalines available from different vendors. Together with the necessary presence of the quinoxaline moiety, the selection was based on in silico prediction/calculation of molecular properties and on molecular similarity to the two active quinoxalines **1** and **2**. With biological tests six hits were identified: in particular, compounds **7** and **8**, bearing a quinazoline and triazolo-quinoxalinic core, showed an interesting inhibitory cell growth activity, even better than 5-FU in the same assay. Further compound selection was carried out by means of substructure searches; although the toxicity of the derivatives, the data collected allowed to refine the optimization which finally led to the three compounds **23**, **24** and **25**, with a reduced toxicity with respect to the starting compounds, while maintaining a similar or even better cytotoxicity.

The data here presented indicate that compound **24** represents the best compromise between antitumor activity and toxicity (selectivity) of drugs with this kind of chemical structure. Compound **23** shares with **24** folate cycle inhibition and similar cytotoxic activity, but not selectivity. Interestingly, unlike 5-FU, both **23** and **24** down-regulate TS expression without inducing ternary complex formation.

The cellular activity profile was studied in detail for the optimized compounds **23–25**, and compared with 5-FU. It has been reported that resistance to 5-FU is due to the up-regulation of TS expression following the binding of inhibitors, as well as of the substrate and the co-substrate, to TS protein causing its dissociation from TS mRNA and thus relieving the translation repression brought about by the TS monomer, allowing translation and increased intracellular TS protein level.[56] In our cell model, the formation of a ternary complex was evident in both lines but it is amplified by the resistant phenotype. In addition, 5-FU treatment derepressing translation accounted for the outstanding level of the ternary complex. According to the suggestion that even the enzyme stabilization could play a role in the induction of TS, as already proposed in other cell lines,[57] 5-FU treatment increased TS protein half-life in both lines.[20]

It is worth noting that **23** and **24** do not induce over-expression of the TS, but instead they lower the protein production, while 5-FU induces TS over-expression in different tumor cell models, including the cell lines used in this study. In addition, **23** and **24** showed a cytotoxic profile similar to **1** and **2** in 2008 and C13* cells, even if to a lower extent. Indeed, **23** and **24** displayed a slight collateral sensitivity against resistant C13* line that correlated with the greater reduction of TS catalytic activity with respect to 2008 parental line. The same correlation was observed for the reduction of DHFR expression. Compound **25** showed a K_i value of 3 μM against hDHFR and the best cellular profile because it is more cytotoxic, even better than 5-FU and less toxic against Vero cells and presumably shares the same cellular effect with respect to **23** and **24** which did not show any inhibition of hDHFR.

Despite the direct correlation between cytotoxic effects and folate cycle enzymes down-regulation is evident, it cannot be ruled out that these quinoxaline compounds may act by affecting different mechanisms other than the folate cycle. In this regard, other quinoxalines structurally similar to those presented here have been reported to act as topoisomerase II poisons and anticancer agents.[58]

Besides, these quinoxalines also showed to affect the intracellular redox state by inducing ROS production, but only in sensitive lines because resistant phenotypes counteract this mechanism.

Another possible mechanism may involve c-Met kinases, a member of receptor tyrosine kinase (RTK) family that is important for normal mammalian development, and found deregulated in high tumor grade,[59] becoming an attractive target for cancer therapy. In this regard, a novel series of quinoxalines as inhibitors

of c-Met kinase has been discovered very recently:[60] this series, structurally similar to the series presented here, indicates an additional likely intracellular target.

Therefore, while characterizing the folate cycle inhibition effect, for these triazolo-quinoxaline compounds other additional inhibition mechanisms cannot be excluded. Thus, the most active and interesting compounds of this series deserve further investigational studies to elucidate in detail all their biochemical target(s).

As a final remark, this work represents an example in which the cellular activity of the compounds, and not the recombinant protein inhibition, guided the drug discovery process and led to the identification of optimized compounds. This approach, differing from the classical enzyme activity guided selection, can be usefully applied when preliminary data clearly shows poor correlation of cellular activity and enzyme inhibition profile.

4. Experimental

4.1. Purity of tested compounds

Purity of compounds was >95%, as determined by TLC. Compounds **1** and **2** were synthesized as reported in Section 4.2. Compounds **3**, **5**, **8**, and **11** were purchased from Chembridge;[61] compounds **4**, **19**, **20**, and **25** from Specs;[62] compounds **6**, **12**, **13** from Chemdiv;[63] compounds **7**, **17**, **18**, **23** and **24** from Key Organics Ltd;[64] compound **9** from Ambinter;[65] compounds **10**, **14**, **15**, **16**, **21** and **22** from Enamine.[66] Compound codes from the vendors are available in the Supplementary data. Compound purity has been defined by TLC using 5:5 ethyl acetate–*n*Exane or 9:1 ethyl acetate–*n*Exane. LCMS for compounds **17**, **18**, **19**, **21**, **22**, **23**, **24**, and **25** are reported as Supplementary data; all of them are LC–MS pure.

4.2. Synthesis

Compounds **1** and **2** were synthesized following the reported methods.[67–71]

4.3. Computational modeling

4.3.1. Flap

The program FLAP[28,29] (Fingerprint for Ligands And Proteins) was originally conceived as a fast algorithm for performing virtual screening by means of a fingerprint-type description of both ligands and protein binding sites. It was designed to describe molecules and protein structures in terms of a common reference framework. This framework can be built from information obtained from the active site of the protein of interest, in which case the resulting study is called a structure-based study, or from ligands which are known to be active for a certain biological target, in which case the resulting study is called a ligand-based study. In ligand-based virtual screening, compounds from virtual libraries are ranked according to their similarity toward a given reference molecule, called a template.[28,29] Given the 3D structure of a molecule, with the GRID force-field[42–44] the interaction energy between the molecule and a probe are calculated at different points in space. As a result, one has the so-called Molecular Interaction Fields (MIF): the hydrophobic and hydrogen bonding interactions of the molecule with a virtual receptor are schematised by the probes and encoded into energy values assigned to the nodes of a grid built around each molecule. MIF are of central importance in the execution of the FLAP algorithm since, given two molecules, their MIF are used by FLAP to align one to the other. The first step of the FLAP procedure is the creation of a database: all the molecules imported will be referred to as ligand molecules. The ligand molecules are subjected to a fast conformational analysis, a reasonable number of conformations are generated and each conformer is individually treated (in this application, up to 50 conformations were generated by FLAP). Some representative fields are extracted from the MIFs of the individual elements entered, and stored in the database. Then, a molecular template is imported, the corresponding MIF are calculated with the program GRID and again some representative fields are selected from the MIFs. The pairwise similarity is calculated on the basis of MIF superposition which, in turn, is obtained by combining quadruplets of hotspots, that could be either molecular atoms or points from the MIF. The first case was used: FLAP classifies all the heavy atoms of ligand molecules as hydrophobic, hydrogen bond donating or accepting, and positively or negatively charged; then FLAP describes each molecule as a set of quadruplets, derived by combining all the hotspots, four by four, in an exhaustive way. Each quadruplet is defined by the character of its composing hotspots, by their six inter-atomic distances, measured in Angstroms and binned in 1 Å intervals, and by an additional flag for the chirality of the quadruplet. The huge information obtained is then documented in a fingerprint mode where the absence or presence of all quadruplets corresponds to 0 or 1, respectively. For computational reasons, only present quadruplets are stored in such a way that facilitates further searches and uses: the information obtained for the template molecule is stored in a virtual bit-string making future computations much easier and quicker to complete and compare. The next step in the FLAP process would be finding the matches of the 4-hotspots of the individual ligands to those of the template. When four hotspots of the ligand molecule are found to fit over four hotspots of the template framework, a potentially favorable superposition has been detected. The process is iterative, and it continues until all the template quadruplets are combined in all possible ways with all ligand quadruplets. Each time, a score associated to the two molecules and their common quadruplet of hotspots quantifies the overlap of the two MIFs: a score is assigned to the superposition in order to evaluate its 'goodness' of MIF-overlapping, using the MIF of the two molecules produced with the GRID probes DRY and OH2. At the end of the process, only the best superposition of each ligand to each template is memorized. Some details of the FLAP calculations are briefly listed: (1) The tolerance between pair wise atoms (from template and ligand molecules) was set to 1 Å. (2) The conformers are produced by FLAP on-the-fly with a routine that randomly modifies the molecule and adds a new conformation to the set only when it differs from the ones already existing. The difference is calculated by using RMSD (root mean square deviation) criteria, using 0.1 as threshold for considering two conformations enough diverse to be treated individually. In this way, the FLAP conformational sampling guarantees an adequate treatment of molecular flexibility in order to span as much as possible the conformational space. For the templates **1** and **2** the conformational analysis was carried out on-the-fly producing ten different conformations and repeating for each conformation the entire procedure described, whereas up to 50 conformers were generated for each ligand molecule, and the best results obtained among these was the result assigned to the compound. (3) GRID probes DRY and OH2 were used to describe the template and each ligand molecule; in addition, the GRID probe H is used for describing the molecular shape. (4) The molecular atoms were used as hotspots. (5) The level of speed was set to 75%. 'Ligand' molecules were subjected to a fast conformational analysis: a reasonable number of conformations were generated, and each conformer was treated individually. Since the FLAP method has been created for virtual screening projects in order to run over libraries of thousands of compounds, the conformational analysis of FLAP is carried out on-the-fly to span reasonably the conformational space.

4.3.2. Potential toxicity and reactivity filter

Potentially toxic functional groups as well as reactive ones were removed following the suggestions of several authors.[45,46] Therefore, the presence of the following chemical moieties served as criterion for removal: (a) five or more halogen atoms, (b) two or more cyano or nitro groups, (c) epoxide or aziridine, (d) two or more aliphatic esters, (e) 1,2-dicarbonyl groups, (f) sulfonate and phosphonate esters, (g) aldehydes, (h) acyl or sulfonyl halides, (i) anhydrides, and (j) heteroatom-heteroatom single bonds, when not in a cycle or linked to aromatic/olefinic systems.

4.3.3. METASITE

METASITE is a program to predict the site of metabolism of drugs and xenobiotics with a mixed approach, which means that information related to both the structure of the protein and the ligand are combined to provide the site of metabolism (SOM) prediction. In 80% of the cases, METASITE predicted the correct SOM within the top three predicted sites.[49,51] The prediction of the most likely metabolically labile site(s) in a structure of a drug candidate can be relevant to modulate the metabolic stability. Increasing the metabolic stability of a compound can be achieved by replacement of the metabolic 'hot spot' with a metabolically stable substituent, such as a trifluoromethyl group, which will resist CYP-catalyzed oxidation. Vice versa, decreasing the metabolic stability of a compound can be achieved by replacement of metabolically stable substituent with atoms/groups metabolically unstable. Predictions of sites of metabolism (SOM) were done with the version 3.0 of METASITE using the P450 liver model that displays a 'weighted consensus' of the SOM predictions of the main isoforms present in the liver such as CYP3A4, CYP2D6, and CYP2C9 and of other isoforms with minor impact such as CYP1A2, CYP2C19, and CYP2E1. The reactivity contribution was set 'On' and 'Off'. When the reactivity is taken into account ('On') the final ranking for potential metabolic sites is the product of the similarity analysis and the chemical reactivity. In the 'Off' mode, METASITE predicts how the protein orients the compounds in the enzyme active site without considering the reactivity of the atoms.

4.3.4. VOLSURF+

VOLSURF+[32–34] is a program to transform 3D energy maps into molecular descriptors. In the VOLSURF+ procedure, first the GRID[42–44] force field is applied to characterize potential polar and hydrophobic interaction sites around target molecules by the water probe (OH2), the hydrophobic probe (DRY), the hydrogen bonding acceptor carbonyl oxygen probe (O) and hydrogen bonding donor amide nitrogen probe (N1). Afterward, molecular descriptors are calculated from these 3D maps. They refer to molecular size and shape, to hydrophilic and hydrophobic regions and to the balance between them. The descriptors used as filters are the molecular weight, the polar surface area, that is calculated starting via the sum of polar region contributions, and SOLY. The descriptor called SOLY is the projection on a quantitative model for thermodynamic aqueous solubility obtained over more than 1100 different chemical structures. The solubility values are the log[Soly] where Soly is expressed in mol/l at 25 °C. Another relevant molecular descriptor was MetStab that is a quantitative model for metabolic stability in human CYP3A4. The predicted MetStab value corresponds to the metabolic stability of a drug incubated at a fixed concentration for 60 min with a fixed concentration of protein at 37 °C. Compounds with a final concentration greater than or equal to 50% of the corresponding control sample were defined as stable, whereas compounds with final concentrations of less than 50% of the corresponding control were defined as unstable. The used version 1.0.2 comprises 128 molecular descriptors covering biologically relevant properties such as shape, surface and volume, electrostatic forces, hydrogen bonding and lipophilicity. Multivariate statistics methods are present in the VOLSURF+ package and are used to enable a simple and straightforward chemical interpretation of the descriptor matrix. Principal Components Analysis (PCA) is an extremely useful technique to 'summarize' all the information contained in the X-matrix in a more understandable form. PCA works by decomposing the X-matrix as the product of two smaller matrices, which are called the loading and score matrices. The Partial Least Squares (PLS) analysis is a regression technique whose goal is to explain dependent variable(s) Y(s) in terms of the X-matrix, that is composed of VOLSURF+ molecular descriptors.

4.4. Biological testing of virtual hits at the enzyme level

Purification protocol hDHFR: The strain BL21 containing the plasmid with human DHFR gene was grown at 37 °C, 120 rpm in 1000 ml of LB medium containing 100 mg/liter ampicillin. Isopropyl-D-thiogalactoside (IPTG) was added (OD600 = 0.7) to a final concentration of 1 mM for the induction of expression. The pellet was defrozen and resuspended in buffer 10 mM $K_xH_yPO_4$, 1 mM EDTA (pH 7.5) using 2 mL/g. The protein was precipitated using $(NH_4)_2SO_4$ 35% and resuspended in buffer 10 mM $K_xH_yPO_4$, 1 mM EDTA (pH 7.5) then dialyzed with buffer 10 mM $K_xH_yPO_4$, 1 mM EDTA (pH 7.5). The resuspended protein was loaded in DE52 column, washed with buffer 10 mM $K_xH_yPO_4$, 1 mM EDTA (pH 7.5). The column was eluted with a gradient from buffer 10 mM $K_xH_yPO_4$, 1 mM EDTA (pH 7.5) to buffer 100 mM $K_xH_yPO_4$, 1 mM EDTA (pH 7.5). The fractions were collected and $(NH_4)_2SO_4$ 1.4 M was added to the pool that was Loaded in Phenyl-Sepharose CL-4B column. The protein was eluted with a gradient from buffer 25 mM $K_xH_yPO_4$, 20 mM βME (pH 7.5) 1.4 M $(NH_4)_2SO_4$ to the buffer 25 mM $K_xH_yPO_4$, 20 mM βME (pH 7.5) 0.5 M $(NH_4)_2SO_4$.

4.4.1. Purification protocol hTS

The strain BL21 containing the plasmid with human TS gene was growth at 37 °C, 120 rpm in 1000 ml of LB medium containing 100 mg/liter ampicillin. Isopropyl-D-thiogalactoside (IPTG) was then added (OD600 = 0.7) to a final concentration of 1 mM for the induction of expression. The pellet was resuspended with buffer 20 mM NaH_2PO_4, 30 mM NaCl, pH 7.5. The crude extract was loaded in Ni-HTP column and washed with buffer 20 mM NaH_2PO_4, 30 mM NaCl, 20 mM imidazole at pH 7.5. The protein was eluted with buffer 20 mM NaH_2PO_4, 30 mM NaCl, 1 M imidazole pH 7.5. The purified protein was obtained loading the Ni-HTP eluted protein through a desalting column with buffer 20 mM NaH_2PO_4, 30 mM NaCl, pH 7.5 provided the 90% purified protein (gel electrophoresis purity grade).

4.4.2. TS assay activity

Assay reaction with a final volume of 800 μl, contained 50 mM TES, 25 mM $MgCl_2$, 6,5 mM formalin, 1 mM EDTA, 75 mM βME, hTS 0.4 μM, mTHF 50 μM, dUMP 120 μM. The reaction was initiated by dUMP followed by rapid shaking. The activity was determined by following the increase of absorbance at λ = 340 nm on a Beckman DU640. The inhibition is performed at maximum compound concentration (0, 50 and 100 μM), depending on compound solubility. The compounds were dissolved in 10 mM DMSO stock.

4.4.3. DHFR assay activity

Assay reaction with a final volume of 800 μl, contained 50 mM TES, 25 mM $MgCl_2$, 6.5 mM formalin, 1 mM EDTA, 75 mM βME, hDHFR 0.5 μM, DHF 50 μM, NADPH 120 μM. The reaction was initiated by NADPH followed by rapid shaking. The activity was determined by following the decrease of absorbance at λ = 340 nm on a Beckman DU640. The inhibition is performed at maximum concentration possible (0, 50 and 100 μM), depending on compound solubility. The compounds were dissolved in 10 mM DMSO stock.

4.5. Biological testing of virtual hits at the cell level

For screening the biological activities of the selected compounds, their effects on different cell lines were studied.

4.5.1. Cell lines

The 2008 cell line was established from a patient with serous cystadenocarcinoma of the ovary and the cDDP-resistant C13* subline, about 15-fold resistant to cDDP, was derived from the parent 2008 cell line by monthly exposure to cDDP, followed by chronic exposure to step-wise increases in cDDP concentration.[72] The human ovarian carcinoma A2780/CP cells are 12-fold resistant to cDDP and derived from the parent A2780 cell line. These human ovarian cell lines were grown as monolayers in RPMI 1640 medium (Lonza, Verviers, Belgium) containing 10% heat-inactivated fetal bovine serum (Lonza, Verviers, Belgium) and 50 μg/ml gentamycin sulfate. Vero cells, established from kidney cells of the African green monkey (Cercopithecus aethiops),[73] were chosen as a control cell line.[21] These cells were obtained from the Istituto Zooprofilattico (Brescia, Italy), and maintained in MEM medium (Whittaker Bioproducts, Walkersville, MD, USA) supplemented with 10% heat-inactivated fetal calf serum (Gibco/BRL, Gaithersburg, MD, USA) and penicillin G (100 μg/ml), streptomycin (100 μg/ml) (Sigma Chemical Company, MO, USA). Human fibroblasts were obtained from healthy donors and cultured in DMEM containing 10% heat-inactivated fetal bovine serum and 50 μg/ml gentamycin sulfate. Cultures were equilibrated with humidified 5% CO_2 in air at 37 °C. The medium was renewed at 48 h intervals, and the cells were always subcultured when the monolayers become confluent. All studies were performed in *Mycoplasma* negative cells, as routinely determined with the *Mycotest* detection kit (Euroclone, Switzerland).

4.5.2. Protein determination

Protein content in the various assays was estimated by the method of Lowry et al.,[74] unless otherwise indicated.

4.5.3. Cell growth assay

Cell growth was determined by a modification of the crystal violet dye assay.[75] Cells were seeded into 24-well plates and allowed to attach overnight, then were treated with proper concentrations of drugs. On selected days, after removal of the tissue culture medium, the cell monolayer was fixed and stained with 0.2% crystal violet solution in 20% methanol for at least 30 min. After washing several times with distilled water to remove the dye excess, the cells were let to dry. The incorporated dye was solubilized in acidic isopropanol (1 N HCl/2-propanol, 1:10). After appropriate dilution, dye was determined spectrophotometrically at 540 nm. The extracted dye was proportional to cell number. Percentage of cytotoxicity was calculated by comparing the absorbance of exposed to non-exposed (control) cultures.

4.5.4. TS catalytic assay

Cells to be used for the enzyme assay were harvested by trypsinization when they were in an exponential growth phase, washed with PBS and used daily or stored at −20 °C for few days. Cell pellets were thawed by the addition of ice-cold lysis buffer (200 mM Tris–HCl pH 7.4, 20 mM 2-mercaptoethanol, 100 mM NaF and 1% Triton X-100), sonicated (three times 5 s with intervals of 5 s), and subsequently centrifuged at 14,000*g* for 15 min at 4 °C. The supernatant was used for enzyme assay. TS catalytic assay, conducted essentially according to a previously reported method,[76] determines the catalytic activity of TS by measuring the amounts of ^3H release from [5-^{3}H]dUMP during its TS catalyzed conversion to dTMP. Briefly, the assay consisted of enzyme suspensions in assay buffer (lysis buffer without Triton X-100), 650 μM 5,10-methylenetetrahydrofolate in a final volume of 50 μl. The reaction was started by adding [5-^{3}H]dUMP (1 μM final concentration, specific activity 5 mCi/mol), incubated for 60 min at 37 °C, and stopped by adding 50 μl of ice-cold 35% trichloroacetic acid. Residual [5-^{3}H]dUMP was removed by the addition of 250 μl of 10% neutral activated charcoal. The charcoal was removed by centrifugation at 14,000*g* for 15 min at 4 °C, and a 150-μl sample of the supernatant was assayed for tritium radioactivity by liquid scintillation counting in the liquid scintillator analyzer Tri-Carb 2100 (Packard). For each cell line, linearity of [5-^{3}H]dUMP conversion with respect to amount of protein and time was established.

4.5.5. Western blotting

Western blot analysis was conducted as previously described.[77] Cells were harvested, washed twice in ice-cold 1× PBS, and resuspended in 20 mM Tris–HCl (pH 7.4), 150 mM NaCl, 1 mM EDTA (pH 8.0), 1% Triton X-100, and 0.1% SDS. Cells were lysed by freeze-thawing three times followed by sonication using three 2-to-3-s bursts. The insoluble debris was removed by centrifugation at 15,000*g* for 30 min. Protein concentrations were determined using the method of Lowry et al.[74] Twenty-five microgram of each protein sample were resolved by SDS–PAGE (12%). The gels were electroblotted onto hydrophobic polyvinylidene difluoride membranes (Hybond™-P PVDF, GE Healthcare Bio-Science, Uppsala, Sweden). Antibody staining was performed with a chemiluminescence detection system (ECL Plus Western Blotting Detection Reagent, GE Healthcare Bio-Science, Uppsala, Sweden), using a 1:500 dilution of the anti-human TS mouse TS106 monoclonal primary antibody (Invitrogen S.r.L., Milan, Italy), 1:1000 dilutions of the anti-human DHFR mouse monoclonal antibody (Tebu-Bio, Milan, Italy) and 1:1000 of anti-human ß-tubulin mouse antibody (Sigma-Aldrich S.r.L., Milan, Italy) in conjunction with a 1:3000 dilution of a horseradish peroxidase-conjugated sheep anti-mouse secondary antibody (GE Healthcare Bio-Science, Uppsala, Sweden). Quantitation of signal intensity was performed by densitometry on a GS-800 calibrated densitometer (Bio-Rad) and analyzed by using Quantity One software (Bio-Rad, CA, USA).

4.5.6. Measurement of reactive oxygen species (ROS) production

Cells were seeded in 96-well plates and treated with drugs for 72 h. 10 μM CM-H2DCFDA, (5-(6) chloromethyl-2′,7′-dichlofluorescein diacetate acetyl ester), (Invitrogen S.r.L., Milan, Italy) was applied for 10 min, in the dark at 37 °C.[55] Afterward, cells were washed and incubated in PBS for 30 min. The amount of ROS, normalized to cell growth by a modification of the crystal violet dye assay, was estimated using the wavelengths of 485 nm (excitation) and 535 nm (emission) in a Tecan GENios Pro (Tecan Trading AG, Switzerland) plate reader. Results were analyzed using Magellan Standard 5.0 software.

4.5.7. Statistical analysis

All values report the mean ± S.E., unless otherwise indicated. Statistical significance was estimated by a two-tailed Student's *t*-test performed using Microsoft Excel Software; a P value <0.05 was considered significant.

Acknowledgments

Supported by LIGHTS, a STREP project within the 6FP (LIGand to Interfere with Human TS, LSHC-CT-2006-037852; www.lights-eu.org), by a grant from COFIN06 (2006030430_004, MIUR, Italy), from Associazione Angela Serra per la Ricerca sul Cancro, Azienda Ospedaliera Policlinico di Modena, Modena, Italy, and partially by PRIN (Programmi di Ricerca Scientifica di Rilevante Interesse Nazionale) 2004, MIUR, Italy.

Supplementary data

Supplementary data associated with this article can be found, in the online version, at doi:10.1016/j.bmc.2010.09.065. These data include MOL files and InChiKeys of the most important compounds described in this article.

References and notes

1. Ozols, R. F.; Daly, M. B.; Klein-Szanto, A.; Hamilton, T. C.; Bast, R. C., Jr.; Brewer, M. A. *Gynecol. Oncol.* **2003**, *88*, S59.
2. Muggia, F. *Gynecol. Oncol.* **2009**, *112*, 275.
3. Scanlon, K. J.; Kashani-Sabet, M. *Proc. Natl. Acad. Sci. U.S.A.* **1988**, *85*, 650.
4. Dickgreber, N. J.; Fink, T. H.; Latz, J. E.; Hossain, A. M.; Musib, L. C.; Thomas, M. *Clin. Cancer Res.* **2009**, *15*, 382.
5. Scagliotti, G. V.; Parikh, P.; von Pawel, J.; Biesma, B.; Vansteenkiste, J.; Manegold, C.; Serwatowski, P.; Gatzemeier, U.; Digumarti, R.; Zukin, M.; Lee, J. S.; Mellemgaard, A.; Park, K.; Patil, S.; Rolski, J.; Goksel, T.; de Marinis, F.; Simms, L.; Sugarman, K. P.; Gandara, D. *J. Clin. Oncol.* **2008**, *26*, 3543.
6. van Meerbeeck, J. P. *J. Thorac. Oncol.* **2006**, *1*, 279.
7. Morgan, R. J.; Braly, P.; Leong, L.; Shibata, S.; Margolin, K.; Somlo, G.; McNamara, M.; Longmate, J.; Schinke, S.; Raschko, J.; Nagasawa, S.; Kogut, N.; Najera, L.; Johnson, D.; Doroshow, J. H. *Gynecol. Oncol.* **2000**, *77*, 433.
8. Araki, H.; Fukushima, M.; Kamiyama, Y.; Tetsuhiko, S. *Cancer Lett.* **2000**, *160*, 185.
9. Kelland, L. R.; Kimbell, R.; Hardcastle, A.; Aherne, G. W.; Jackman, A. L. *Eur. J. Cancer* **1995**, *31A*, 981.
10. Scanlon, K. J.; Newman, E. M.; Lu, Y.; Priest, D. G. *Proc. Natl. Acad. Sci. U.S.A.* **1986**, *83*, 8923.
11. Newman, E. M.; Lu, Y.; Kashani-Sabet, M.; Kesavan, V.; Scanlon, K. J. *Biochem. Pharmacol.* **1988**, *37*, 443.
12. Lu, Y.; Han, J.; Scanlon, K. J. *J. Biol. Chem.* **1988**, *263*, 4891.
13. Lai, G. M.; Ozols, R. F.; Smyth, J. F.; Young, R. C.; Hamilton, T. C. *Biochem. Pharmacol.* **1988**, *37*, 4597.
14. Wang, L.; Cherian, C.; Desmoulin, S. K.; Polin, L.; Deng, Y.; Wu, J.; Hou, Z.; White, K.; Kushner, J.; Matherly, L. H.; Gangjee, A. *J. Med. Chem.* **2010**, *53*, 1306.
15. Tomao, F.; Panici, P. B.; Frati, L.; Tomao, S. *Expert Rev. Anticancer Ther.* **2009**, *9*, 1727.
16. Sehouli, J.; Camara, O.; Mahner, S.; Bauknecht, T.; Lichtenegger, W.; Runnebaum, I.; Look, K.; Jaenicke, F.; Oskay-Oezcelik, G. *Cancer Chemother. Pharmacol.* **2010**. doi:10.1007/s00280-009-1230-3.
17. Carreras, C. W.; Santi, D. V. *Ann. Rev. Biochem.* **1995**, *64*, 721.
18. Costi, M. P.; Ferrari, S. *Curr. Drug Targets* **2001**, *2*, 135.
19. Carta, A.; Corona, P.; Loriga, M. *Curr. Med. Chem.* **2005**, *12*, 2259.
20. Marverti, G.; Ligabue, A.; Paglietti, G.; Corona, P.; Piras, S.; Vitale, G.; Guerrieri, D.; Luciani, R.; Costi, M. P.; Frassineti, C.; Moruzzi, M. S. *Eur. J. Pharmacol.* **2009**, *615*, 17.
21. Rossi, T.; Coppi, A.; Bruni, E.; Ruberto, A.; Santachiara, S.; Baggio, G. *Anticancer Res.* **2007**, *27*, 2555.
22. Menezo, Y. J. R.; Guerin, J. F.; Czyba, J. C. *Biol. Reprod.* **1990**, *42*, 301.
23. Marverti, G.; Ligabue, A.; Guerrieri, D.; Paglietti, G.; Piras, S.; Costi, M. P.; Farina, D.; Frassineti, C.; Monti, M. G.; Moruzzi, M. S. *Gynecol. Oncol.* **2010**, *117*, 202.
24. Gao, H.; Yamasaki, E. F.; Chan, K. K.; Shen, L. L.; Snapka, R. M. *Mol. Pharmacol.* **2003**, *63*, 1382.
25. Irwin, J. J.; Shoichet, B. K. *J. Chem. Inf. Model.* **2005**, *45*, 177.
26. http://zinc.docking.org.
27. Stahura, F. L.; Bajorath, J. *Curr. Pharm. Des.* **2005**, *11*, 1189.
28. Baroni, M.; Cruciani, G.; Sciabola, S.; Perruccio, F.; Mason, J. S. *J. Chem. Inf. Model.* **2007**, *47*, 279.
29. Cross, S.; Baroni, M.; Carosati, E.; Benedetti, P.; Clementi, S. *J. Chem. Inf. Model.* **2010**, *50*, 1442.
30. Weininger, D. *J. Chem. Inf. Comput. Sci.* **1988**, *28*, 31.
31. Weininger, D.; Weininger, A.; Weininger, J. L. *J. Chem. Inf. Comput. Sci.* **1989**, *29*, 97.
32. Cruciani, G.; Crivori, P.; Carrupt, P.-A.; Testa, B. *J. Mol. Struct. – Theochem.* **2000**, *503*, 17.
33. Crivori, P.; Cruciani, G.; Carrupt, P.-A.; Testa, B. *J. Med. Chem.* **2000**, *43*, 2204.
34. The VOLSURF+ program, version 1.0.2, is distributed by Molecular Discovery Ltd, http://www.moldiscovery.com.
35. The Flap program is distributed by Molecular Discovery Ltd, http://www.moldiscovery.com.
36. Sciabola, S.; Stanton, R. V.; Mills, J. E.; Flocco, M. M.; Baroni, M.; Cruciani, G.; Perruccio, F.; Mason, J. S. *J. Chem. Inf. Model.* **2010**, *50*, 155.
37. Carosati, E.; Cruciani, G.; Chiarini, A.; Budriesi, R.; Ioan, P.; Spisani, R.; Spinelli, D.; Cosimelli, B.; Fusi, F.; Frosini, M.; Matucci, R.; Gasparrini, F.; Ciogli, A.; Stephens, P. J.; Devlin, F. J. *J. Med. Chem.* **2006**, *49*, 5206.
38. Carosati, E.; Mannhold, R.; Wahl, P.; Hansen, J. B.; Fremming, T.; Zamora, I.; Cianchetta, G.; Baroni, M. *J. Med. Chem.* **2007**, *50*, 2117.
39. Sciabola, S.; Carosati, E.; Cucurull-Sanchez, L.; Baroni, M.; Mannhold, R. *Bioorg. Med. Chem.* **2007**, *15*, 6450.
40. Budriesi, R.; Cosimelli, B.; Ioan, P.; Ugenti, M. P.; Carosati, E.; Frosini, M.; Fusi, F.; Spisani, R.; Saponara, S.; Cruciani, G.; Novellino, E.; Spinelli, D.; Chiarini, A. *J. Med. Chem.* **2009**, *52*, 2352.
41. Carosati, E.; Budriesi, R.; Ioan, P.; Cruciani, G.; Fusi, F.; Frosini, M.; Saponara, S.; Gasparrini, F.; Ciogli, A.; Villani, C.; Stephens, P. J.; Devlin, F. J.; Spinelli, D.; Chiarini, A. *J. Med. Chem.* **2009**, *52*, 6637.
42. Goodford, P. J. *J. Med. Chem.* **1985**, *28*, 849.
43. Carosati, E.; Sciabola, S.; Cruciani, G. *J. Med. Chem.* **2004**, *47*, 5114.
44. The GRID package, version 22, is distributed by Molecular Discovery Ltd, http://www.moldiscovery.com.
45. Rishton, G. M. *Drug Discovery Today* **1997**, *2*, 382.
46. Olah, M. M.; Bologa, C. G.; Oprea, T. I. *Curr. Drug Discov. Technol.* **2004**, *1*, 211.
47. Bernauer, U.; Heinrich-Hirsch, B.; Tönnies, M.; Peter-Matthias, W.; Gundert-Remy, U. *Toxicol. Lett.* **2006**, *164*, 278.
48. Oyama, T.; Sugio, K.; Uramoto, H.; Kawamoto, T.; Kagawa, N.; Nadaf, S.; Carbone, D.; Yasumoto, K. *Front* **2007**, *12*, 2299.
49. Androutsopoulos, V. P.; Tsatsakis, A. M.; Spandidos, D. A. *BMC Cancer* **2009**, *9*, 187.
50. Cruciani, G.; Carosati, E.; De Boeck, B.; Ethirajulu, K.; Mackie, C.; Howe, T.; Vianello, R. *J. Med. Chem.* **2005**, *48*, 6970.
51. The METASITE program, version 3.0.0, is distributed by Molecular Discovery Ltd, http://www.moldiscovery.com.
52. Ahlström, M. M.; Ridderström, M.; Zamora, I.; Luthman, K. J. *J. Med. Chem.* **2007**, *50*, 4444.
53. Ahlström, M. M.; Ridderström, M.; Zamora, I. *J. Med. Chem.* **2007**, *50*, 5382.
54. Chen, Y.; Kramer, D. L.; Diegelman, P.; Vujcic, S.; Porter, C. W. *Cancer Res.* **2001**, *61*, 6437.
55. Marzano, C.; Gandin, V.; Folda, A.; Scutari, G.; Bindoli, A.; Rigobello, M. P. *Free Radical Biol. Med.* **2007**, *42*, 872.
56. Chu, E.; Koeller, D. M.; Casey, J. L.; Drake, J. C.; Chabner, B. A.; Elwood, P. C.; Zinn, S.; Allegra, C. J. *PNAS* **1991**, *88*, 8977.
57. Kitchens, M. E.; Forsthoefel, A. M.; Barbour, K. W.; Spencer, H. T.; Berger, F. G. *Mol. Pharmacol.* **1999**, *56*, 1063.
58. Gao, H. L.; Huang, K. C.; Yamasaki, E. F.; Chan, K. K.; Chohan, L.; Snapka, R. M. *Proc. Natl. Acad. Sci. U.S.A.* **1999**, *96*, 12168.
59. Birchmeier, C.; Birchmeier, W.; Gherardi, E.; van de Woude, G. F. *Nat. Rev. Mol. Cell Biol.* **2003**, *4*, 915.
60. Porter, J.; Lumb, S.; Lecomte, F.; Reuberson, J.; Foley, A.; Calmiano, M.; le Riche, K.; Edwards, H.; Delgado, J.; Franklin, R. J.; Gascon-Simorte, J. M.; Maloney, A.; Meier, C.; Batchelor, M. *Bioorg. Med. Chem. Lett.* **2009**, *19*, 397.
61. http://chembridge.com.
62. http://www.specs.net.
63. http://www.chemdiv.com.
64. http://www.keyorganics.co.uk.
65. http://www.ambinter.com.
66. http://www.enamine.net.
67. Loriga, M.; Fiore, M.; Sanna, P.; Paglietti, G. *Il Farmaco* **1995**, *50*, 289.
68. Loriga, M.; Moro, P.; Sanna, P.; Paglietti, G. *Il Farmaco* **1997**, *52*, 531.
69. Loriga, M.; Piras, S.; Paglietti, G.; Costi, M. P.; Venturelli, A. *Il Farmaco* **2003**, *58*, 51.
70. Piras, S.; Loriga, M.; Paglietti, G. *Il Farmaco* **2004**, *59*, 185.
71. Piras, S.; Loriga, M.; Carta, A.; Paglietti, G.; Costi, M. P.; Ferrari, S. *J. Heterocycl. Chem.* **2006**, *43*, 541.
72. Andrews, P. A.; Albright, K. D. *Cancer Res.* **1992**, *52*, 1895.
73. Bianchi, N. O.; Ayres, J. *Exp. Cell Res.* **1971**, *68*, 253.
74. Lowry, O. H.; Rosebrough, N. J.; Farr, A. L.; Randall, R. J. *J. Biol. Chem.* **1951**, *193*, 265.
75. Kueng, W.; Siber, E.; Eppenberger, U. *Anal. Biochem.* **1989**, *182*, 16.
76. van Triest, B.; Pinedo, H. M.; van Hensbergen, Y.; Smid, K.; Telleman, F.; Schoenmakers, P. S.; van der Wilt, C. L.; van Laar, J. A. M.; Noordhuis, P.; Jansen, G.; Peters, G. J. *Clin. Cancer Res.* **1999**, *5*, 643.
77. Longley, D. B.; Ferguson, P. R.; Boyer, J.; Latif, T.; Lynch, M.; Maxwell, P.; Harkin, D. P.; Johnston, P. G. *Clin. Cancer Res.* **2001**, *7*, 3533.